# Real-Time Identifiability of Power Distribution Network Topologies with Limited Monitoring

Guido Cavraro, Andrey Bernstein, Vassilis Kekatos, and Yingchen Zhang

***Abstract*—Recovering the distribution grid topology in real time is essential to perform several distribution system operator (DSO) functions. DSOs often do not have any direct monitoring of switch statuses to track reconfiguration. At the same time, installing real-time meters at a large number of buses is challenging due to the cost of endowing every metered bus with a real-time communication channel. The goal of this paper is to develop a meter placement strategy allowing DSOs to deploy only few real-time meters. After casting the topology recovery task as an optimization problem, a meter placement strategy ensuring unique recovery of the true topology is devised. A graph-theoretical approach is pursued to partition the grid into connected portions called *observable islands*. The proposed strategy then simply requires installing a meter in the path between every pair of *boundary nodes*, i.e., ends of edges connecting two different islands. Under some ideal assumptions, this placement strategy ensures unique recovery of the topology. The approach is also validated through numerical simulations under realistic scenarios using a standard IEEE benchmark feeder.**

***Index Terms*—Energy systems; identification; smart grid.**

## I. Introduction

DISTRIBUTION grid topology identification has become a timely research topic. On one hand, the massive deployment of distributed resources challenges the operation of distribution networks calling for the development of advanced control, optimization, and monitoring solutions [1]. These tasks cannot be performed without knowing the grid topology. On the other hand, the knowledge of the network topology is fundamental during grid restoration after a disruptive event [2].

Prior work on unveiling feeder topologies builds on second-order statistics of grid data; see, e.g., [3]. Graphical models have been used to fit a spanning tree relying on the mutual information of voltage data [4]. Tree recovery methods operating in both a bottom-up and a top-down fashion have been devised in [5], [6], [7]. In [8], topology recovery has been cast as a maximum likelihood problem. Although topology identification has been considered for power transmission systems [9], [10], exploiting the radial nature of distribution grids can simplify topology detection schemes.

Smart meters transmit data to DSOs periodically on a 15- or 60-min basis, a reporting mode that might be insufficient to detect grid reconfigurations in a timely manner. Therefore, real-time data are necessary to identify the actual grid topology. Unfortunately, distribution grids have limited real-time metering infrastructure, due to the high cost of endowing every bus with real-time metering and of establishing a reliable real-time communication link between metered buses and the utility. Hence, it is crucial to devise allocation strategies of real-time meters that enable the DSOs to recover the grid topology exploiting the least number of sensors.

Typically, DSOs know the underlying physical structure, i.e., lines connecting buses and their parameters [6], [8], [11]. However, beside fixed lines that are always energized, there are *switching lines*, also termed *switches*, that, depending if they are energized or not, set the actual grid topology. In this letter, we consider the problem of identifying the energized lines based on limited real-time information and some statistical properties of the grid. First, we cast the problem as an optimization problem aiming at identifying the status of switching lines and consequently at recovering the network topology. Second, we propose a sensor placement strategy that guarantees, under some commonly adopted assumptions, that the status of switches can be uniquely recovered. The developed strategy uses the second-order statistics built over historical power data to extract all the information needed to recover the grid topology. Finally, the meter placement strategy is tested numerically on an IEEE benchmark feeder.

## II. Modeling Preliminaries

### A. Electric Grid Modeling

A radial single-phase distribution grid having $N+1$ buses can be modeled by a graph $\mathcal{G} = (\mathcal{V}^+, \mathcal{L})$. Nodes in the set $\mathcal{V}^+$ correspond to buses, and edges in $\mathcal{L}$ to distribution lines. Index the substation by 0, and collect the remaining $N$ buses in set $\mathcal{V}$, so that $\mathcal{V}^+ = \mathcal{V} \cup \{0\}$. Define $v_n$ and $p_n + jq_n$ as the voltage magnitude (henceforth voltage) and complex power injected at bus $n$. Collect the voltages and the power injections observed at $\mathcal{V}$ in vectors $(\mathbf{v}, \mathbf{p}, \mathbf{q})$. From the $L := |\mathcal{L}|$ edges, the subset $\mathcal{S} \subseteq \mathcal{L}$ of cardinality $S := |\mathcal{S}|$ corresponds to switches, i.e., lines that can be switched on/off. Let $r_\ell + jx_\ell$ be the impedance of line $\ell \in \mathcal{L}$, and stack all impedances in $\mathbf{r} + j\mathbf{x}$. The line infrastructure of the grid can be captured by

Manuscript received March 1, 2019; revised May 14, 2019; accepted June 8, 2019. This work was supported in part by the National Renewable Energy Laboratory (NREL), operated by Alliance for Sustainable Energy, LLC, for the U.S. Department of Energy under Contract DE-AC36-08GO28308, in part by the Laboratory Directed Research and Development Program at NREL, and in part by NSFCAREER under Grant 1751085. The views expressed in the paper do not necessarily represent the views of the DOE or the U.S. Government. The publisher, by accepting the paper for publication, acknowledges that the U.S. Government retains a nonexclusive, paid-up, irrevocable, worldwide license to publish or reproduce the published form of this work, or allow others to do so, for U.S. Government purposes. Recommended by Senior Editor R. S. Smith. (Corresponding author: Guido Cavraro.)

G. Cavraro, A. Bernstein, and Y. Zhang are with the Power Systems Engineering Center, National Renewable Energy Laboratory, Golden, CO 80401 USA (e-mail: name.surname@nrel.gov). V. Kekatos is with the Bradley Department of ECE, Virginia Tech, Blacksburg, VA 24061 USA (e-mail: kekatos@vt.edu).

Digital Object Identifier 10.1109/LCSYS.2019.2926101

the branch-bus incidence matrix $\tilde{\mathbf{A}} \in \{0, \pm 1\}^{L \times N}$. Matrix $\tilde{\mathbf{A}}$ can be partitioned as $\tilde{\mathbf{A}} = [\mathbf{a}_0 \ \mathbf{A}]$, with $\mathbf{a}_0$ being the column associated with the substation. Distribution networks usually operate in a radial fashion. The operational topology of the grid is determined by the switches in $\mathcal{S}$. Let $w_s$ be a binary variable capturing the status of switch $s$, and collect all $w_s$'s in vector $\mathbf{w}$. Denote as $\mathcal{R}$ the set of *admissible configurations*, that is the values of $\mathbf{w}$ yielding radial and connected networks.

Voltage magnitudes are nonlinearly related to power injections. Yet, we adopt a grid model derived upon linearizing the power flow equations (see [8], [3], or [12])

$$\mathbf{v} = \mathbf{R}(\mathbf{w})\mathbf{p} + \mathbf{X}(\mathbf{w})\mathbf{q} + \mathbf{1}. \tag{1}$$

where $\mathbf{R}(\mathbf{w})$ and $\mathbf{X}(\mathbf{w}) \in \mathbb{R}^{N \times N}$ are defined as

$$\mathbf{R}^{-1}(\mathbf{w}) := \sum_{\ell \in \mathcal{S}} \frac{w_\ell}{r_\ell} \mathbf{a}_\ell \mathbf{a}_\ell^\top + \sum_{\ell \in \mathcal{L} \setminus \mathcal{S}} \frac{1}{r_\ell} \mathbf{a}_\ell \mathbf{a}_\ell^\top \tag{2a}$$

$$\mathbf{X}^{-1}(\mathbf{w}) := \sum_{\ell \in \mathcal{S}} \frac{w_\ell}{x_\ell} \mathbf{a}_\ell \mathbf{a}_\ell^\top + \sum_{\ell \in \mathcal{L} \setminus \mathcal{S}} \frac{1}{x_\ell} \mathbf{a}_\ell \mathbf{a}_\ell^\top \tag{2b}$$

and $\mathbf{a}_\ell^\top$ is the $\ell$-th row of $\mathbf{A}$. The first (second) summations in the RHS of (2) capture the contribution of switches (lines). The inverses exist for all $\mathbf{w} \in \mathcal{R}$; see [13].

Let $\mathcal{O} \subseteq \mathcal{V}$ with $O := |\mathcal{O}|$, be the set of buses metered in real time, or simply *metered buses*. For these buses, the DSO collects voltage and power readings in real time. The remaining buses comprise the set of non real-time metered buses, or simply *non-metered buses*, $\mathcal{N} := \mathcal{V} \setminus \mathcal{O}$. Non-metered buses periodically send packets of smart meter data hourly or three times a day [14]. Because multiple topology changes might occur within the same day, real-time data are necessary to detect the current grid configuration in a timely fashion. Without loss of generality, let us partition nodal variables by grouping together metered and non-metered buses as

$$\mathbf{v}^\top = [\mathbf{v}_\mathcal{O}^\top \ \ \mathbf{v}_\mathcal{N}^\top]; \quad \mathbf{p}^\top = [\mathbf{p}_\mathcal{O}^\top \ \ \mathbf{p}_\mathcal{N}^\top]; \quad \mathbf{q}^\top = [\mathbf{q}_\mathcal{O}^\top \ \ \mathbf{q}_\mathcal{N}^\top]$$

where the subscripts $\mathcal{O}$ and $\mathcal{N}$ identify the subset of vector entries corresponding to the two sets of buses. Matrix $\mathbf{R}(\mathbf{w})$ (similarly $\mathbf{X}(\mathbf{w})$ too) can be partitioned conformably as

$$\mathbf{R}(\mathbf{w}) = \left[\begin{array}{c|c} \mathbf{R}_{\mathcal{O}\mathcal{O}}(\mathbf{w}) & \mathbf{R}_{\mathcal{O}\mathcal{N}}(\mathbf{w}) \\ \hline \mathbf{R}_{\mathcal{N}\mathcal{O}}(\mathbf{w}) & \mathbf{R}_{\mathcal{N}\mathcal{N}}(\mathbf{w}) \end{array}\right] = \left[\begin{array}{c} \mathbf{R}_{\mathcal{O}}(\mathbf{w}) \\ \hline \mathbf{R}_{\mathcal{N}}(\mathbf{w}) \end{array}\right] \tag{3}$$

Let $\mathbf{S}_\mathcal{O} \in \{0,1\}^{O \times N}$ be the selection matrix obtained from $\mathbf{I}_N$ by keeping only the rows corresponding to $\mathcal{O}$. Based on this selection matrix, we can compactly express the subvector $\mathbf{v}_\mathcal{O} = \mathbf{S}_\mathcal{O}\mathbf{v}$, and the matrix blocks $\mathbf{R}_{\mathcal{O}\mathcal{O}}(\mathbf{w}) = \mathbf{S}_\mathcal{O}\mathbf{R}(\mathbf{w})\mathbf{S}_\mathcal{O}^\top$ and $\mathbf{R}_\mathcal{O}(\mathbf{w}) = \mathbf{S}_\mathcal{O}\mathbf{R}(\mathbf{w})$. Likewise for $\mathbf{X}_{\mathcal{O}\mathcal{O}}$ and $\mathbf{X}_\mathcal{O}$.

### B. Graphs and Distribution Grids

Let $\mathcal{G}(\mathbf{w}) = (\mathcal{V}, \mathcal{E}(\mathbf{w}))$ be the undirected graph representing the energized topology associated with the edge statuses $\mathbf{w}$. A *path* in a tree graph is the unique sequence of edges connecting two nodes. The set of nodes adjacent to the edges forming the path between nodes $n$ and $m$ is denoted by $\mathcal{P}_{n,m}(\mathbf{w})$. The *ancestors* of node $m$ are defined as the nodes belonging to $\mathcal{A}_m(\mathbf{w}) := \mathcal{P}_{0,m}(\mathbf{w})$. A node $m$ is a *descendant* of node $n$ if $n \in \mathcal{A}_m(\mathbf{w})$. The descendants of node $m$ are collected in set $\mathcal{D}_m(\mathbf{w})$; see also Fig. 1. By convention, it holds that $m \in \mathcal{A}_m(\mathbf{w})$ and $m \in \mathcal{D}_m(\mathbf{w})$. If $n \in \mathcal{A}_m(\mathbf{w})$ and $(m,n) \in \mathcal{E}$, node $n$ is the *parent* of $m$. The *depth* $d_m(\mathbf{w})$ of node $m$ is defined as the number of its ancestors $d_m(\mathbf{w}) := |\mathcal{A}_m(\mathbf{w})|$. If $n \in \mathcal{A}_m(\mathbf{w})$ and $d_n = k$, node $n$ is the unique $k$-depth ancestor of node $m$ and will be denoted by $\alpha_m^k(\mathbf{w})$ for $k = 0, \ldots, d_m$. Due to the tree structure of $\mathcal{G}(\mathbf{w})$, the entries of $\mathbf{R}(\mathbf{w})$ exhibit an interesting property [6]: To find the $(m,n)$-th entry of $\mathbf{R}(\mathbf{w})$, one has to draw the paths from buses $m$ and $n$ to the substation, identify the overlapping edges, and sum up the resistances over these edges, that is

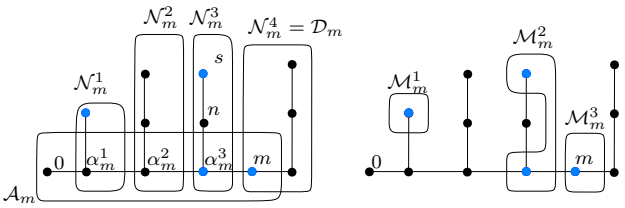


Fig. 1. The left panel shows the ancestor $\mathcal{A}_m$ and descendant $\mathcal{D}_m$ sets for node $m$. It also shows its level sets $\mathcal{N}_m^1, \mathcal{N}_m^2, \mathcal{N}_m^3$, and $\mathcal{N}_m^4$. The right panel shows the metered level sets for node $m$ if metered buses are colored blue.

$$[\mathbf{R}(\mathbf{w})]_{mn} = \sum_{\substack{(c,d) \in \mathcal{L} \\ c,d \in \mathcal{A}_m(\mathbf{w}) \cap \mathcal{A}_n(\mathbf{w})}} r_{c,d}. \tag{4}$$

Define the *$k$-th level set* of node $m$ as [13]

$$\mathcal{N}_m^k(\mathbf{w}) := \begin{cases} \mathcal{D}_{\alpha_m^k}(\mathbf{w}) \setminus \mathcal{D}_{\alpha_m^{k+1}}(\mathbf{w}) & , \ k = 0, \ldots, d_m - 1 \\ \mathcal{D}_m(\mathbf{w}) & , \ k = d_m. \end{cases}$$

Level set $\mathcal{N}_m^k$ consists of bus $\alpha_m^k$ and the tree rooted at $\alpha_m^k$ excluding the subtree containing node $m$; see Fig. 1. Finally, the $k$-th *metered level set* of $m \in \mathcal{O}$ is defined as [7]

$$\mathcal{M}_m^k(\mathbf{w}) = \mathcal{N}_m^{h_k}(\mathbf{w}) \cap \mathcal{O}, \tag{5}$$

where $h_0 = 0$, and $h_k = \min\{j \in \{h_{k-1}, \ldots, d_m\} : \mathcal{N}_m^j \cap \mathcal{O} \neq \emptyset\}$. In words, $\mathcal{N}_m^{h_k}(\mathbf{w})$ is the $k$-th level set having at least one observed node, see Fig. 1. The next result, proved in the Appendix, relates metered level sets and entries of $\mathbf{R}_{\mathcal{O}\mathcal{O}}(\mathbf{w})$.

**Proposition 1.** *Let $m, n, s$ be metered nodes on a tree $\mathcal{G}(\mathbf{w})$:*

1) *Nodes $n$ and $s$ belong to the same metered level set $\mathcal{M}_m^k(\mathbf{w})$ if and only if $[\mathbf{R}_{\mathcal{O}\mathcal{O}}(\mathbf{w})]_{mn} = [\mathbf{R}_{\mathcal{O}\mathcal{O}}(\mathbf{w})]_{ms}$*
2) *if $[\mathbf{R}_{\mathcal{O}\mathcal{O}}(\mathbf{w})]_{mn} < [\mathbf{R}_{\mathcal{O}\mathcal{O}}(\mathbf{w})]_{ms}$, then $n$ and $s$ belong to different metered level sets, i.e., $n \in \mathcal{M}_m^{k'}, s \in \mathcal{M}_m^{k''}$, with $k' < k''$.*

A direct consequence of Proposition 1 is presented next.

**Corollary 1.** *Consider two switch configurations $\mathbf{w}$ and $\mathbf{w}' \in \mathcal{R}$. If there exists a node $m$ and a level $k \leq d_m$ such that $\mathcal{M}_m^k(\mathbf{w}) \neq \mathcal{M}_m^k(\mathbf{w}')$, then $\mathbf{R}_{\mathcal{O}\mathcal{O}}(\mathbf{w}) \neq \mathbf{R}_{\mathcal{O}\mathcal{O}}(\mathbf{w}')$.*

Prop. 1, Cor. 1, and (4) carry over to matrix $\mathbf{X}_{\mathcal{O}\mathcal{O}}$ as well.

## III. Topology Recovery

Given voltage and power injection data at metered buses, the goal is to identify the actual switch status vector denoted by $\mathbf{w}_0 \in \mathcal{R}$. Upon postulating a statistical model on the collected

data, this section poses this task as an optimization problem. Rather than using voltage and power injections directly, our method relies on *differential* voltage and power injections $\tilde{\mathbf{v}}(t) := \mathbf{v}(t) - \mathbf{v}(t-1), \tilde{\mathbf{p}}(t) := \mathbf{p}(t) - \mathbf{p}(t-1), \tilde{\mathbf{q}}(t) := \mathbf{q}(t) - \mathbf{q}(t-1)$. From (1), differential data are related as

$$\tilde{\mathbf{v}}(t) = \mathbf{R}(\mathbf{w})\tilde{\mathbf{p}}(t) + \mathbf{X}(\mathbf{w})\tilde{\mathbf{q}}(t). \tag{6}$$

Working with differential data eliminates vector $\mathbf{1}$ from the RHS of (1) and justifies the ensuing statistical modeling.

**Assumption 1.** *Differential power injections* $\{\tilde{\mathbf{p}}(t), \tilde{\mathbf{q}}(t)\}_t$ *are*

p1) *zero-mean random vectors* $\mathbb{E}[\tilde{\mathbf{p}}(t)] = \mathbb{E}[\tilde{\mathbf{q}}(t)] = \mathbf{0}$*;*

p2) *uncorrelated across time*

$$\mathbb{E}[\tilde{\mathbf{p}}(t)\tilde{\mathbf{p}}^\top(\tau)] = \delta_{t,\tau}\mathbf{\Sigma}_p\mathbf{I}_N, \mathbb{E}[\tilde{\mathbf{q}}(t)\tilde{\mathbf{q}}^\top(\tau)] = \delta_{t,\tau}\mathbf{\Sigma}_q\mathbf{I}_N \tag{7a}$$

$$\mathbb{E}[\tilde{\mathbf{p}}(t)\tilde{\mathbf{q}}^\top(\tau)] = \delta_{t,\tau}\mathbf{\Sigma}_{pq}\mathbf{I}_N \tag{7b}$$

*where* $\delta_{t,\tau}$ *is the Kronecker delta function;*

p3) *uncorrelated across buses, that is the covariance matrices* $\mathbf{\Sigma}_p$*,* $\mathbf{\Sigma}_q$*, and* $\mathbf{\Sigma}_{pq}$ *are diagonal. We will further presume* $\mathbf{\Sigma}_p = \sigma_p^2\mathbf{I}_N$*;* $\mathbf{\Sigma}_q = \sigma_q^2\mathbf{I}_N$*; and* $\mathbf{\Sigma}_{pq} = \sigma_{pq}\mathbf{I}_N$*, although our analysis holds for general diagonal matrices.*

The former properties serve as good approximations of true differential power injections, especially for sampling rates in the order of seconds or minutes: Properties p1) and p2) are extensively tested on real data in [8] and [15]. Assumption p3) is commonly assumed in the literature [3], [5], [8], [12]. The diagonal entries of $\mathbf{\Sigma}_p$, $\mathbf{\Sigma}_q$, and $\mathbf{\Sigma}_{pq}$ can be readily estimated using historical data collected from both metered and non-metered buses. Despite Assumption 1, heed that the numerical tests are performed using real-world power injections.

Real-time differential voltage and power injection data are gathered by the utility from the buses in $\mathcal{O}$ over times $t = 1, \ldots, T$. The following set of measurements is available

$$\left\{\tilde{\mathbf{v}}_\mathcal{O}(t) + \boldsymbol{\epsilon}_v(t), \tilde{\mathbf{p}}_\mathcal{O}(t) + \boldsymbol{\epsilon}_p(t), \tilde{\mathbf{q}}_\mathcal{O}(t) + \boldsymbol{\epsilon}_q(t)\right\}_{t=1}^T \tag{8}$$

where $\boldsymbol{\epsilon}_v(t)$, $\boldsymbol{\epsilon}_p(t)$, and $\boldsymbol{\epsilon}_q(t)$ are errors capturing measurement noise, modeling approximations, and unmodeled dynamics. These noise vectors are modeled as iid Gaussian random vectors, independent across time and buses with respective variances $\gamma_v^2$, $\gamma_p^2$, and $\gamma_q^2$, common to all buses.

The *topology detection task* amounts to finding the actual switch status $\mathbf{w}_0$ given the line infrastructure $\{\mathbf{a}_\ell, r_\ell, x_\ell\}_{\ell\in\mathcal{E}}$; the covariances $\mathbf{\Sigma}_p$, $\mathbf{\Sigma}_q$, $\mathbf{\Sigma}_{pq}$; the set $\mathcal{O}$; and the data in (8).

Based on the preceding modeling, collected data meet

$$\tilde{\mathbf{v}}_\mathcal{O}(t) = \mathbf{R}_\mathcal{O}(\mathbf{w}_0)\tilde{\mathbf{p}}(t) + \mathbf{X}_\mathcal{O}(\mathbf{w}_0)\tilde{\mathbf{q}}(t) \tag{9}$$

and their ensemble covariance matrices can be computed as

$$\tilde{\mathbf{\Sigma}}_v = \mathbb{E}[\tilde{\mathbf{v}}_\mathcal{O}\tilde{\mathbf{v}}_\mathcal{O}^\top] = \mathbf{R}_\mathcal{O}\mathbf{\Sigma}_p\mathbf{R}_\mathcal{O}^\top + \mathbf{R}_\mathcal{O}\mathbf{\Sigma}_{pq}\mathbf{X}_\mathcal{O}^\top + \mathbf{X}_\mathcal{O}\mathbf{\Sigma}_{pq}^\top\mathbf{R}_\mathcal{O}^\top + \mathbf{X}_\mathcal{O}\mathbf{\Sigma}_q\mathbf{X}_\mathcal{O}^\top + \gamma_v^2\mathbf{I}_\mathcal{O} \tag{10a}$$

$$\tilde{\mathbf{\Sigma}}_{vp} = \mathbb{E}[\tilde{\mathbf{v}}_\mathcal{O}\tilde{\mathbf{p}}_\mathcal{O}^\top] = \mathbf{R}_\mathcal{O}\mathbf{\Sigma}_p\mathbf{S}_\mathcal{O}^\top + \mathbf{X}_\mathcal{O}\mathbf{\Sigma}_{pq}^\top\mathbf{S}_\mathcal{O}^\top \tag{10b}$$

$$\tilde{\mathbf{\Sigma}}_{vq} = \mathbb{E}[\tilde{\mathbf{v}}_\mathcal{O}\tilde{\mathbf{q}}_\mathcal{O}^\top] = \mathbf{R}_\mathcal{O}\mathbf{\Sigma}_{pq}\mathbf{S}_\mathcal{O}^\top + \mathbf{X}_\mathcal{O}\mathbf{\Sigma}_q\mathbf{S}_\mathcal{O}^\top. \tag{10c}$$

whose dependence on $\mathbf{w}_0$ through $\mathbf{R}_\mathcal{O}(\mathbf{w}_0)$ and $\mathbf{X}_\mathcal{O}(\mathbf{w}_0)$ has been suppressed in (10) for notational simplicity. Let $\hat{\mathbf{\Sigma}}_v$, $\hat{\mathbf{\Sigma}}_{vp}$, $\hat{\mathbf{\Sigma}}_{vq}$ be the sample counterparts of the covariance matrices in (10), computed from the data collected in real time in (8). For example, matrix $\hat{\mathbf{\Sigma}}_v$ is defined as $\hat{\mathbf{\Sigma}}_v := \frac{1}{T}\sum_{t=1}^T \tilde{\mathbf{v}}_\mathcal{O}(t)\tilde{\mathbf{v}}_\mathcal{O}^\top(t)$.

After defining $f_v(\mathbf{w}) = \|\tilde{\mathbf{\Sigma}}_v(\mathbf{w}) - \hat{\mathbf{\Sigma}}_v\|_F^2$; $f_p(\mathbf{w}) := \|\tilde{\mathbf{\Sigma}}_{vp}(\mathbf{w}) - \hat{\mathbf{\Sigma}}_{vp}\|_F^2$; and $f_q(\mathbf{w}) := \|\tilde{\mathbf{\Sigma}}_{vq}(\mathbf{w}) - \hat{\mathbf{\Sigma}}_{vq}\|_F^2$, we state the topology recovery problem as

$$\mathbf{w}^* := \arg\min_{\mathbf{w}\in\mathcal{R}} f_v(\mathbf{w}) + f_p(\mathbf{w}) + f_q(\mathbf{w}). \tag{11}$$

The solution $\mathbf{w}^*$ is the configuration that best matches the sample covariance matrices with their ensemble versions. The goal of problem (11) is to extract from the second order data statistics the information about the current grid topology. Leveraging this interpretation, problem (11) can be seen as a generalization of topology recovery tasks proposed in the literature, e.g., reference [8] aims at finding $\mathbf{w}^*$ given the voltage sample covariance. As in [12], if the term $f_v(\mathbf{w})$ is dropped in (11), then one needs to compute only the diagonal entries of $\mathbf{\Sigma}_p$, $\mathbf{\Sigma}_q$, and $\mathbf{\Sigma}_{pq}$ corresponding to metered buses.

Problem (11) is a nonconvex combinatorial optimization task. Here, we assume that the space $\mathcal{R}$ is sufficiently small so that (11) can be solved via exhaustive enumeration. As an example, the set $\mathcal{R}$ associated with the 37-bus feeder reported in Sec. V counts only eight elements. Rather than focusing on efficient solutions to (11), we are interested in selecting metered buses $\mathcal{O}$ to ensure that the actual $\mathbf{w}_0$ is identifiable.

## IV. Sensor Placement for Topology Recovery

To study if the actual switch status vector $\mathbf{w}_0$ is the unique minimizer of (11), it is assumed that the sample covariance matrices have converged to their ensemble values, that is

$$\hat{\mathbf{\Sigma}}_v = \tilde{\mathbf{\Sigma}}_v(\mathbf{w}_0), \quad \hat{\mathbf{\Sigma}}_{vp} = \tilde{\mathbf{\Sigma}}_{vp}(\mathbf{w}_0), \quad \hat{\mathbf{\Sigma}}_{vq} = \hat{\mathbf{\Sigma}}_{vq}(\mathbf{w}_0). \tag{12}$$

This is a standard assumption in identifiability analysis, and is widely adopted in grid topology recovery [3], [5], [7], [12], [13]. Before stating the meter placement strategy, let us introduce some additional elements from graph theory.

Consider a graph $\mathcal{G} = (\mathcal{V}, \mathcal{L})$. and partition $\mathcal{V}$ into connected sets of nodes $\{\mathcal{V}_i\}$ such that $\mathcal{V} = \oplus_i\mathcal{V}_i$. Let $\mathcal{G}_i = (\mathcal{V}_i, \mathcal{L}_i)$ be the subgraph of $\mathcal{G}$ where $\mathcal{L}_i = \{(m,n) \in \mathcal{L}; m, n \in \mathcal{V}_i\}$. An *island graph* $\mathcal{H} = (\mathcal{I}, \mathcal{F})$ is a graph such that [11]:

- Every node $i \in \mathcal{I}$ is associated with a subgraph $\mathcal{G}_i$ and is termed *island*. An island can be equivalently denoted by $\mathcal{G}_i$ or $i$. The substation is contained in island $\mathcal{G}_1$.
- Edge $f = (i,j) \in \mathcal{F}$ if and only if there exists an arc in $\mathcal{L}$ connecting a node in $\mathcal{G}_i$ with a node in $\mathcal{G}_j$. With a slight abuse of notation, we can say that $\mathcal{F} = \mathcal{L}\backslash(\cup_i\mathcal{L}_i)$. In a sense, every $f \in \mathcal{F}$ is a *bridge* connecting two islands.

To state our placement strategy, we define an *observable island graph* $\mathcal{H}_o = (\mathcal{I}_o, \mathcal{F}_o)$ as an island graph such that

- Every switch $s \in \mathcal{S}$ is an edge in $\mathcal{F}_o$. That is, with a slight abuse of notation, $\mathcal{S} \subseteq \mathcal{F}_o$; and
- Two nodes $i, j \in \mathcal{I}_o$ are linked by at most one edge.

Some illustrative examples of island graphs and observable island graphs are shown in Fig. 2. The connectivity among islands in $\mathcal{I}_o$ is a function of the switch status: every $\mathbf{w} \in \mathcal{R}$ defines a set of energized edges $\mathcal{F}_o(\mathbf{w}) \subset \mathcal{F}_o$ and, consequently, the island graph $\mathcal{H}(\mathbf{w}) = (\mathcal{I}_o, \mathcal{F}_o(\mathbf{w}))$; see Fig. 3.

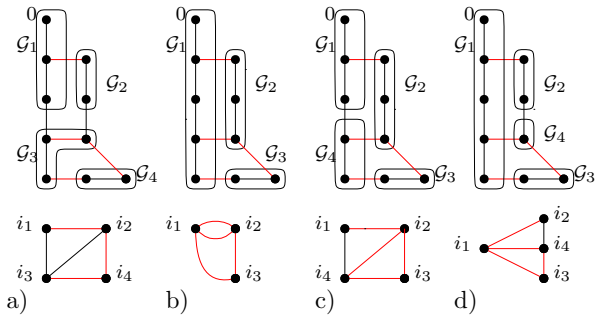


Fig. 2. Black and red arcs denote fixed lines and switches, respectively. *a)* A graph is partitioned into four connected subgraphs. The resulting island graph has four nodes. *b)* The graph is partitioned into islands divided by switches. $\mathcal{G}_1$ and $\mathcal{G}_2$ are connected by two edges. Hence the resulting island graph is not an observable island graph. *c)* Island $\mathcal{G}_1$ is further partitioned to obtain $\mathcal{G}_4$. The resulting graph is an observable island graph. *d)* A different observable island graph is obtained by further partitioning $\mathcal{G}_2$ instead of $\mathcal{G}_1$.

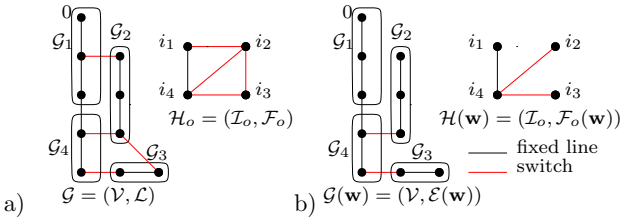


Fig. 3. Panel a) shows an observable island graph $\mathcal{H}_o$ built on $\mathcal{G}$. The island graph $\mathcal{H}(\mathbf{w})$ determined by the switch status $\mathbf{w}$ is depicted in panel b).

Observe that $\mathcal{H}(\mathbf{w})$ is always a subgraph of $\mathcal{H}_o$. Furthermore, $\mathcal{H}(\mathbf{w})$ is always a tree rooted at $i_1$, the island containing the substation. Given the special structure of the observable island graph, namely, all the switches of the distribution network $\mathcal{G}$ are edges in $\mathcal{F}_o$, it turns out that if $\mathbf{w} \neq \mathbf{w}'$ then $\mathcal{H}(\mathbf{w}) \neq \mathcal{H}(\mathbf{w}')$. Consider island $\mathcal{G}_i$ of an observable island graphs, and let it be connected with other islands by the arcs $f_1 = (m_1, n_1), \ldots, f_c = (m_c, n_c)$, $f_1, \ldots, f_c \in \mathcal{F}_o$. Nodes $m_1, \ldots, m_c \in \mathcal{G}_i$ constitute the set of boundary nodes of $\mathcal{G}_i$. Include the substation among the boundary nodes of $\mathcal{G}_1$.

**Definition 1.** *A set of metered nodes $\mathcal{O}$ is said to meet the* observable meter placement strategy *(OMPS) if there is a metered bus in the path between every pair of boundary nodes, for every island $\mathcal{G}_i$; see Fig. 4.*

The next theorem provides the features of the OMPS.

**Theorem 1.** *Let $\mathcal{G} = (\mathcal{V}, \mathcal{L})$ be the graph representing the physical infrastructure of a distribution grid. Let $\mathcal{H}_o = (\mathcal{I}_o, \mathcal{F}_o)$ be an observable island graph derived form $\mathcal{G}$ and let $\mathcal{O}$ be a set of metered buses. If $\mathcal{O}$ meets the OMPS, then*

*1) given $\mathbf{w}$ and $i, j \in \mathcal{I}_o$, $i \in \mathcal{D}_j$, all the nodes in $\mathcal{G}_i$ are descendants of a bus $m$ in island $\mathcal{G}_j$, see Fig. 5, i.e.,*

$$\exists\, m \in \mathcal{G}_i : n \in \mathcal{D}_m(\mathbf{w}),\ \forall n \in \mathcal{G}_j, \tag{13}$$

*2) $\mathbf{w}_0$ is identifiable, i.e., it is the only solution of* (11).

Given the physical underlying infrastructure, it is simple to partition the electric grid into an observable island graph. Thus, a sensor placement meeting the OMPS can be easily

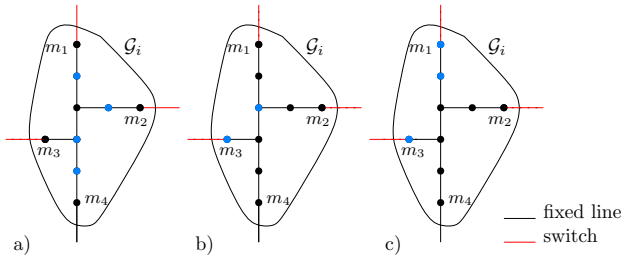


Fig. 4. Three placements of metered buses (blue nodes) are reported. Configurations in a) and b) meet the OMPS, while c) do not. Note that the number of metered nodes can be reduced by smartly placing them.

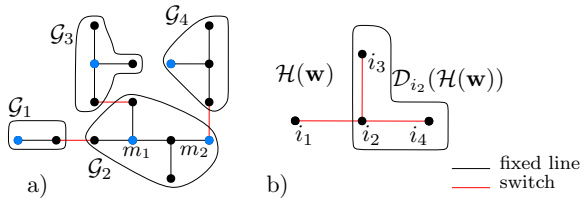


Fig. 5. Panel a) reports metered nodes (blue nodes) placed meeting the OMPS. Panel b) depicts the island graph $\mathcal{H}(\mathbf{w})$. Heed that all nodes of $\mathcal{G}_3$ are descendants of $m_1$, while all nodes of $\mathcal{G}_4$ are descendants of $m_2$.

obtained. Results on meter allocation have already appeared in the literature, where it has been shown that retrieving data from leaf (terminal) nodes suffices to detect the grid topology, e.g., see [6]. On the other hand, Theorem 1 does not provide neither the minimum number of meters that guarantees the identifiability of $\mathbf{w}_0$, nor an automatic way to deploy the sensors. However, if sensors are allocated smartly, their number can be kept very small compared to the other aforementioned strategy, as we will show in Section V.

## V. Numerical Tests

The modified IEEE 37-bus feeder depicted in Fig. 6 was used for our numerical tests; see [13] for the details. The feeder can operate under eight distinct radial topologies, i.e., $\mathcal{R}$ have eight elements. In every simulation, the switch status was randomly picked from $\mathcal{R}$. An observable island graph was found by dividing the testbed into six islands; see Fig. 6. Real-world residential data were collected from the Pecan Street project for January 1, 2013 [16]. These data were used as load power profiles and to build the diagonal power covariances in (10). Voltages were obtained through a full AC power flow solver; see [8] for the details on data generation.

The topology recovery performance using the next meter placements was tested. The set $\mathcal{O}^6_{obs} = \{12, 17, 23, 26, 30, 33\}$ is the placement satisfying the OMPS condition with the smaller number of meters (one sensor per island). Placement $\mathcal{O}^{12}_{obs} = \{2, 5, 11, 12, 14, 17, 20, 22, 23, 26, 30, 33\}$ endows every island with two meters. In $\mathcal{O}^6_{rand}$ and $\mathcal{O}^{12}_{rand}$ six and twelve sensors, respectively, are deployed randomly. In $\mathcal{O}_{all}$, all buses are metered. Other placement policies would require installing a meter on every possible leaf node [5], [7], i.e., 16 meters.

First, problem (11) was solved under the ideal setup (IS) used for the identifiability analysis of Section IV: voltages and power injections obeyed (6); Assumption 1 was met; and

TABLE I
TOPOLOGY AND SWITCH ERROR PROBABILITIES (TEP/SEP)

| | | IS | $T = 24$ | 48 | 72 | 96 | 120 |
|---|---|---|---|---|---|---|---|
| $\mathcal{O}^6_{obs}$ | TEP [%] | 0 | 11.2 | 5.7 | 4.5 | 4.2 | 3.4 |
| | SEP [%] | 0 | 24.2 | 13.4 | 11.6 | 11.2 | 7.6 |
| $\mathcal{O}^{12}_{obs}$ | TEP [%] | 0 | 6.3 | 4.4 | 3.2 | 2.9 | 2.8 |
| | SEP [%] | 0 | 13.4 | 9.0 | 7.6 | 8.2 | 6.6 |
| $\mathcal{O}_{all}$ | TEP [%] | 0 | 3.3 | 3.2 | 3.0 | 3.0 | 2.7 |
| | SEP [%] | 0 | 9.0 | 7.6 | 8.6 | 7.6 | 6.2 |
| $\mathcal{O}^6_{rand}$ | TEP [%] | 5.6 | 30.8 | 24.8 | 23.2 | 19.9 | 19.0 |
| | SEP [%] | 8.8 | 72.4 | 53.0 | 51.6 | 43.4 | 42.2 |
| $\mathcal{O}^{12}_{rand}$ | TEP [%] | 1.9 | 15.1 | 11.1 | 10.6 | 10.4 | 10.2 |
| | SEP [%] | 3.8 | 35.8 | 24.0 | 24.6 | 23.4 | 22.6 |

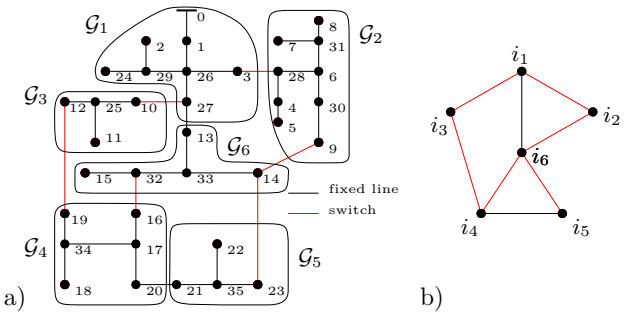


Fig. 6. Panel a) reports the IEEE 37-bus distribution feeder with six switches. Panel b) reports the observable island graph built over the testbed.

sample covariances were set to their ensemble counterparts. The third column of Table I collects the topology error probability (TEP) and the switch error probability (SEP), computed after $1,000$ Monte Carlo tests. According to Proposition 1, placements $\mathcal{O}^6_{obs}$, $\mathcal{O}^{12}_{obs}$ and $\mathcal{O}_{all}$ yielded no errors.

Second, a realistic setup was considered. Problem (11) was solved for different numbers of collected data samples $T$, ranging from 24 to 120, and a sampling period of $T_s = 5$ min in $1,000$ Monte Carlo runs. The results are reported in Table I, columns 4-8. Not surprisingly, performance improves as the number of available samples or deployed meters increases. In fact, the better results provided by $\mathcal{O}^{12}_{obs}$ over $\mathcal{O}^6_{obs}$ can be explained in terms of available information, since meter readings are collected at twice the number of locations. However, note that $\mathcal{O}^6_{obs}$ outperforms both $\mathcal{O}^6_{rand}$ and $\mathcal{O}^{12}_{rand}$, although the latter used the double number of meters.

## VI. CONCLUSIONS

We proposed a sensor placement strategy to identify the energized grid topology exploiting real-time information collected at only a few buses. Simulations on the standard IEEE-37 bus testbed have shown the effectiveness of the proposed strategy. Generalizations to multi-phase and meshed grids, as well as the integration of distribution PMU data constitute interesting research directions.

## APPENDIX

*Proof of Proposition 1:* Assume that the linearized model of (1) holds true. Based on (4), one can recognize that the entry $[\mathbf{R}]_{mn}$ equals the voltage drop from $v_0$ incurred at bus $n$ when a unitary active power is absorbed at bus $m$, while the remaining buses are unloaded. Kirchoff's current law states that power flows from the substation towards bus $m$ only through the ancestors of $m$. As a consequence, two buses $n$ and $s$ belong to $\mathcal{N}^k_m$ if and only if they are equipotential, since no power is flowing between them, that is

$$v_n = v_s \iff [\mathbf{R}]_{mn} = [\mathbf{R}]_{ms}. \tag{14}$$

On the other hand, if the voltage drop from $v_0$ of $n$ is smaller than the one of $s$, it means that $n$ and $s$ belong to different level sets, i.e., $n \in \mathcal{N}^{h'}_m, s \in \mathcal{N}^{h''}_m$, with $h' < h''$. Proposition 1 claims readily follows from the previous reasoning and from the definition of metered level sets. ■

### A. Proof of Theorem 1

Before proving Th. 1, some claims are needed. Assuming sample statistics have converged to their ensemble counterparts [cf. (12)], let $\Pi$ be the optimal set for (11). $\Pi$ is not empty, since $\mathbf{w}_0 \in \Pi$. Indeed, vector $\mathbf{w}_0$ belongs to $\mathcal{R}$, and also yields a zero objective for (11). Then every $\mathbf{w} \in \Pi$ belongs also to

$$\Pi' := \{\mathbf{w} : f_v(\mathbf{w}) = f_p(\mathbf{w}) = f_q(\mathbf{w}) = 0\} \tag{15}$$

or $\Pi \subseteq \Pi'$. The reverse containment may not hold since not all $\mathbf{w} \in \Pi'$ belong to $\mathcal{R}$. Let us also define the set

$$\Pi'' := \{\mathbf{w} : f_p(\mathbf{w}) = f_q(\mathbf{w}) = 0\} \tag{16}$$

for which $\Pi \subseteq \Pi' \subseteq \Pi''$, and so $\mathbf{w}_0$ belongs to all three sets $\Pi$, $\Pi'$, and $\Pi''$. If we were able to find a meter placement $\mathcal{O}$ that renders $\mathbf{w}_0$ the single element of $\Pi''$, then $\mathbf{w}_0$ would also be the single element of $\Pi$. To avoid pathological situations, we make the following assumption [5].

**Assumption 2.** *For the covariances of differential power injections in* (7)*, it holds that* $\sigma_p\sigma_q \neq |\sigma_{pq}|$.

The following claim should hold for a placement $\mathcal{O}$ to ensure topology identifiability. After that, the main result is proved.

**Lemma 1.** *Under Assumption 2, if the set of metered buses* $\mathcal{O}$ *is such that* $\mathbf{w}_0$ *is the unique solution to*

$$\mathbf{R}_{\mathcal{O}\mathcal{O}}(\mathbf{w}) = \mathbf{R}_{\mathcal{O}\mathcal{O}}(\mathbf{w}_0), \quad \mathbf{X}_{\mathcal{O}\mathcal{O}}(\mathbf{w}) = \mathbf{X}_{\mathcal{O}\mathcal{O}}(\mathbf{w}_0) \tag{17}$$

*then* $\mathbf{w}_0$ *is the unique minimizer of* (11)*.*

*Proof:* From (10b)–(10c), any solution $\mathbf{w}$ to the equations defining $\Pi''$ in (16) should satisfy

$$\sigma_p^2\mathbf{R}_{\mathcal{O}\mathcal{O}}(\mathbf{w}) + \sigma_{pq}\mathbf{X}_{\mathcal{O}\mathcal{O}}(\mathbf{w}) = \sigma_p^2\mathbf{R}_{\mathcal{O}\mathcal{O}}(\mathbf{w}_0) + \sigma_{pq}\mathbf{X}_{\mathcal{O}\mathcal{O}}(\mathbf{w}_0)$$
$$\sigma_{pq}\mathbf{R}_{\mathcal{O}\mathcal{O}}(\mathbf{w}) + \sigma_q^2\mathbf{X}_{\mathcal{O}\mathcal{O}}(\mathbf{w}) = \sigma_{pq}\mathbf{R}_{\mathcal{O}\mathcal{O}}(\mathbf{w}_0) + \sigma_q^2\mathbf{X}_{\mathcal{O}\mathcal{O}}(\mathbf{w}_0).$$

After some manipulations, the previous equations yield

$$(\sigma_{pq}^2 - \sigma_p^2\sigma_q^2)\mathbf{R}_{\mathcal{O}\mathcal{O}}(\mathbf{w}) = (\sigma_{pq}^2 - \sigma_p^2\sigma_q^2)\mathbf{R}_{\mathcal{O}\mathcal{O}}(\mathbf{w}_0)$$
$$(\sigma_{pq}^2 - \sigma_p^2\sigma_q^2)\mathbf{X}_{\mathcal{O}\mathcal{O}}(\mathbf{w}) = (\sigma_{pq}^2 - \sigma_p^2\sigma_q^2)\mathbf{X}_{\mathcal{O}\mathcal{O}}(\mathbf{w}_0).$$

Under Assumption 2, the last equations become equivalent to condition (17). Under the condition in (17), vector $\mathbf{w}_0$ is the unique element of $\Pi''$, and thus, the unique element of $\Pi$. ■

*Proof of Theorem 1:* Consider two islands $i, j \in \mathcal{I}_o$, and let $j$ be the parent of $i$ in $\mathcal{H}(\mathbf{w})$. There exist two buses $m_1, n_1$ that are boundary nodes, respectively, in $\mathcal{G}_j$ and $\mathcal{G}_i$, such that $e_1 = (m_1, n_1) \in \mathcal{E}(\mathbf{w})$. It holds that

$$n \in \mathcal{G}_i \quad \Rightarrow \quad n \in \mathcal{D}_{m_1}(\mathbf{w}). \tag{18}$$

Two cases can be identified: First, there exists an island $h$ such that $h$ is the parent of $j$ in $\mathcal{H}(\mathbf{w})$. In this case, let $m_2, n_2$ denote the boundary nodes belonging to $\mathcal{G}_j$ and $\mathcal{G}_h$, respectively, such that $e_2 = (m_2, n_2) \in \mathcal{E}(\mathbf{w})$. Second, it holds $j = 1$. For this second case, set $m_2 = 0$, that is $m_2$ is the substation. In both cases, let $m$ be a metered node placed in the path between $m_1$ and $m_2$. By construction, it holds

$$m_1 \in \mathcal{D}_m(\mathbf{w}). \tag{19}$$

Equation (13) follows by combining (18) and (19).

Consider a switch configuration $\mathbf{w} \neq \mathbf{w}_0$, so

$$\mathcal{H}(\mathbf{w}) \neq \mathcal{H}(\mathbf{w}_0). \tag{20}$$

We next show that there exists a bus $m$ and a level $k \leq d_m$ such that $\mathcal{M}_m^k(\mathbf{w}) \neq \mathcal{M}_m^k(\mathbf{w}_0)$. Thus, Corollary 1 ensures that $\mathbf{w}$ does not satisfy (17). Proving by contradiction, suppose

$$\mathcal{M}_m^k(\mathbf{w}) = \mathcal{M}_m^k(\mathbf{w}_0), \quad \forall m \in \mathcal{O}, k \leq d_m. \tag{21}$$

Let $\mathcal{U}(\mathbf{w})$ and $\mathcal{U}(\mathbf{w}_0)$ denote the set of leaf nodes of $\mathcal{H}(\mathbf{w})$ and $\mathcal{H}(\mathbf{w}_0)$, respectively. First, equation (21) implies $\mathcal{U}(\mathbf{w}) = \mathcal{U}(\mathbf{w}_0)$. In fact, assume that $i$ is a leaf of $\mathcal{H}(\mathbf{w})$ but not a leaf of $\mathcal{H}(\mathbf{w}_0)$. For any $m \in \mathcal{G}_i \cap \mathcal{O}$

$$(\mathcal{D}_m(\mathbf{w}) \cap \mathcal{O}) = \mathcal{M}_m^{d_m}(\mathbf{w}) \subseteq \mathcal{G}_i \cap \mathcal{O}, m \in \mathcal{G}_i. \tag{22}$$

In words, the metered descendants of $m$ can only be metered nodes of $\mathcal{G}_i$. Since $i$ is a leaf of $\mathcal{H}(\mathbf{w})$ but not a leaf of $\mathcal{H}(\mathbf{w}_0)$, there exists a $j$ such that island $\mathcal{G}_j$ is a descendant of island $\mathcal{G}_i$ in $\mathcal{H}(\mathbf{w}_0)$. Equation (13) guarantees that there exists a metered $m \in \mathcal{G}_i$ such that every node in $\mathcal{G}_j$ is its descendant, that is $\exists\, m \in \mathcal{G}_i : \{n \in \mathcal{G}_j \cap \mathcal{O}\} \in \mathcal{M}_m^{d_m}(\mathbf{w})$, which contradicts (22).

Second, condition (20) implies that there exists an island $i$ and a subtree of $\mathcal{H}(\mathbf{w})$ rooted at $i$, denoted by $\mathcal{T}_i(\mathcal{H}(\mathbf{w}))$, satisfying the properties: *(i)* It appears also in the original graph $\mathcal{H}(\mathbf{w}_0)$, that is $\mathcal{T}_i(\mathcal{H}(\mathbf{w})) = \mathcal{T}_i(\mathcal{H}(\mathbf{w}_0))$; and *(ii)* The line $f = (i, j) \in \mathcal{F}_o(\mathbf{w})$ does not occur in $\mathcal{H}(\mathbf{w}_0)$, i.e., $f \notin \mathcal{F}_o(\mathbf{w}_0)$. Such $\mathcal{T}_i(\mathcal{H}(\mathbf{w}))$ always exists, and it might be for any leaf island $i$ the singleton $\mathcal{T}_i(\mathcal{H}(\mathbf{w})) = \{i\}$. Thanks to (13), if the OSPS is adopted, there exists a node $n \in \mathcal{G}_j \cap \mathcal{O}$ such that the metered descendants of $n$ are exactly $n$ itself and the metered nodes in $\mathcal{G}_i$, see Fig. 7-a), i.e.,

$$\mathcal{M}_n^{d_n}(\mathbf{w}) = \{n\} \cup \left\{ m \in \sum_{k \in \mathcal{T}_i(\mathcal{H}(\mathbf{w}))} \mathcal{G}_k \cap \mathcal{O} \right\}. \tag{23}$$

Now there are two scenarios. In the first scenario, we have $i \notin \mathcal{D}_j(\mathbf{w}_0)$ and then, none of the nodes in $\mathcal{G}_i$ is a descendant of any nodes in $\mathcal{G}_j$, see Fig. 7-b). This implies that

$$m \notin \mathcal{M}_n^{d_n}(\mathbf{w}_0), m \in \mathcal{G}_\ell, \ell \in \mathcal{T}_i(\mathcal{H}(\mathbf{w})). \tag{24}$$

In the second scenario, island $i$ is still a descendant of $j$, but there is at least another island $k$ such that $j$ is the parent of $k$. At this point, there are two additional cases. In the first subcase, the nodes in $\mathcal{G}_k$ are not descendants of $n$, see Fig. 7-c). As a consequence, equation (24) still holds. In the second subcase, the descendants of $n$ consist of metered nodes in $\mathcal{G}_k$ and in $\mathcal{T}_i(\mathcal{H}(\mathbf{w}))$, see also Fig. 7-d), that is

$$\{n\} \cup \{m \in \mathcal{G}_i \cap \mathcal{O}\} \subset \mathcal{M}_n^{d_n}(\mathbf{w}_0). \tag{25}$$

Eq. (24) and (25) contradict (23), thus $\mathcal{M}_n^{d_n}(\mathbf{w}) \neq \mathcal{M}_n^{d_n}(\mathbf{w}_0)$. Lemma 1 implies that $\mathbf{w}_0$ is the unique minimizer of (11). ■

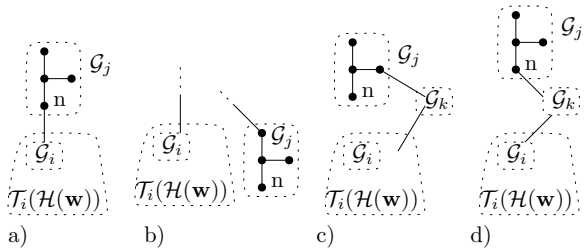


Fig. 7. Pictorial explanation for the proof of Theorem 1.

## REFERENCES


[1] A. Azizivahed, A. Arefi, S. Jirsaraie, M. Shafie-khah, L. Li, J. Zhang, and J. Catalao, "Energy management strategy in dynamic distribution network reconfiguration considering renewable energy resources and storage," *IEEE Trans. Sustain. Energy*, vol. 99, pp. 1–1, 2019.

[2] L. Tang, F. Yang, and J. Ma, "A survey on distribution system feeder reconfiguration: Objectives and solutions," in *Proc. IEEE Conf. on Innovative Smart Grid Technologies*, Kuala Lumpur, Malaysia, May 2014, pp. 62–67.

[3] S. Bolognani, N. Bof, D. Michelotti, R. Muraro, and L. Schenato, "Identification of power distribution network topology via voltage correlation analysis," in *Proc. IEEE Conf. on Decision and Control*, Florence, Italy, Dec. 2013, pp. 1659–1664.

[4] Y. Weng, Y. Liao, and R. Rajagopal, "Distributed energy resources topology identification via graphical modeling," *IEEE Transactions on Power Systems*, vol. 32, no. 4, pp. 2682–2694, July 2017.

[5] S. Park, D. Deka, and M. Chertkov, "Exact topology and parameter estimation in distribution grids with minimal observability," in *Proc. Power Syst. Comput. Conf.*, Dublin, Ireland, Jun. 2018, pp. 1–6.

[6] D. Deka, S. Backhaus, and M. Chertkov, "Learning topology of distribution grids using only terminal node measurements," in *Proc. IEEE Intl. Conf. on Smart Grid Commun.*, Syndey, Australia, Nov. 2016.

[7] G. Cavraro and V. Kekatos, "Graph algorithms for topology identification using power grid probing," *IEEE Control Systems Letters*, vol. 2, no. 4, pp. 689–694, Oct. 2018.

[8] G. Cavraro, V. Kekatos, and S. Veeramachaneni, "Voltage analytics for power distribution network topology verification," *IEEE Trans. Smart Grid*, vol. 10, no. 1, pp. 1058–1067, Jan. 2019.

[9] S. Nabavi and A. Chakrabortty, "Topology identification for dynamic equivalent models of large power system networks," in *Proc. American Control Conf.*, Washington, DC, USA, Jun. 2013, pp. 1138–1143.

[10] V. Kekatos and G. B. Giannakis, "Joint power system state estimation and breaker status identification," in *Proc. North American Power Symposium*, Urbana-Champaign, IL, Sep. 2012, pp. 1–6.

[11] R. A. Sevlian, Y. Zhao, R. Rajagopal, A. Goldsmith, and H. V. Poor, "Outage detection using load and line flow measurements in power distribution systems," *IEEE Trans. Power Syst.*, vol. 33, no. 2, pp. 2053–2069, Mar. 2018.

[12] D. Deka, M. Chertkov, and S. Backhaus, "Structure learning in power distribution networks," *IEEE Trans. Control Netw. Syst.*, vol. 5, no. 3, pp. 1061–1074, Sep. 2018.

[13] G. Cavraro and V. Kekatos, "Inverter probing for power distribution network topology processing," *IEEE Trans. Control Netw. Syst.*, 2019.

[14] W. Luan, D. Sharp, and S. LaRoy, "Data traffic analysis of utility smart metering network," in *Proc. IEEE Power & Energy Society General Meeting*, Vancouver, BC, Canada, Jul. 2013, pp. 1–4.

[15] G. Cavraro and R. Arghandeh, "Power distribution network topology detection with time-series signature verification method," *IEEE Trans. Power Syst.*, vol. 33, no. 4, pp. 3500–3509, July 2018.

[16] (2013) Pecan Street Inc. https://dataport.pecanstreet.org/.